Craze plasticity and toughness of particulate block copolymer blends

O. S. Gebizlioglu*, A. S. Argon*, R. E. Cohen†
Massachusetts Institute of Technology, Cambridge, MA 02139, USA
(Received 13 February 1984; revised 9 July 1984)

Blends of KRO-1 Resin in high molecular weight polystyrene in which the K-Resin appears as dispersed spherical composite particles with the characteristic K-Resin morphology have been modified by incorporating into them additional polybutadiene of a molecular weight of 3 kg/mole (PB3K). It was found that small additions of PB3K into KRO-1 initiate first a morphological transformation resulting in particles with two coexisting morphologies of distorted rods and parallel lamellae. At a ratio of PB3K/KRO-1 of somewhat above 0.33 the transformation is complete and results in composite particles with a very regular concentric spherical shell morphology of PB and PS. The craze initiating effectiveness of composite particles peaks with this morphology, resulting in craze flow stresses as low as 8 MPa and strains to fracture in excess of 0.80 for a PB3K/KRO-1 ratio of 0.5. Larger volume concentrations of PB3K result in reprecipitation of free PB3K inside particles and this gives rise to a rapid degradation of toughness. The very effective craze initiating action of the spherical shell particles cannot be fully accounted for by the best techniques of numerical stress analysis of the elastic and thermal properties of the composite particles utilizing locally multiaxial craze initiation criteria that were developed for surface crazing in homo-PS. It is suspected that the craze initiation condition is locally relaxed around such composite particles by the presence of certain pre-existing 'catalytic' interface configurations that makes the nucleation of crazes from such particle interfaces more a heterogeneous nucleation phenomenon than a homogeneous nucleation phenomenon.

(Keywords: crazing, toughness, composite particles, block copolymers, blending for toughness)

INTRODUCTION

It is now well-known that the incorporation of a certain volume fraction of rubbery composite particles in glassy polymers can impart substantial levels of toughness. In systems for which toughening is predominantly by stable crazing, the accumulated experience has shown that in order to achieve high toughness it is necessary to nucleate and grow a large volume fraction of crazes throughout the volume without permitting either these crazes to transform into cracks or the composite particles to detach from the matrix. For this purpose, it has been necessary to use a high molecular weight glassy polymer for the matrix to assure craze matter stability; to provide an interface with good adhesion between the composite particle and the matrix; and to control particle shape, size and internal structure for a given volume fraction of the rubbery phase. Much of this accumulated know-how has been discussed by Kambour[1] and Bucknall[2].

The rubber-toughened systems are oil-in-oil emulsions[3,4] of graft or block copolymers of a rubbery component and a glassy component, incorporated in a glassy homopolymer of relatively large average molecular weight. Although earlier preparations are almost invariably based on graft copolymerization of a rubber to a glassy polymer matrix, Riess and Jolivet[5], Echte[6] and Kruse[7] have shown that block copolymers can be used to construct particles with a variety of shapes and morphologies.

In the preceding paper of Gebizlioglu *et al.*[8], to be referred to here as (I), we presented the results of our study on toughening by crazing in blends of block copolymers of polybutadiene and polystyrene (PB/PS), in a high molecular weight polystyrene matrix. The films prepared from these blends exhibit particle morphologies characteristic of the block copolymers used. Stereological analyses showed broad-size distributions of composite particles for the two block copolymers of different microstructures. Tensile experiments in combination with transmission electron microscopy (TEM) of the crazed samples have indicated that the principal morphological length scale governed by the smallest dimension of the block copolymer phase, typically of the order of 20 nm, is too small to initiate crazes. Since this dimension can also not be increased readily by an order of magnitude or more, as might be required, by increasing the molecular weight of the individual block components or by ternary blending, other procedures are necessary to control the craze initiating effectiveness of composite particles. On the basis of observations by Bucknall and coworkers[9,10], which have been verified many times[11,12], it is necessary to govern craze initiation conditions over volume elements that exceed a definite critical size, which translates for conventional HIPS particles to diameters in excess of 1–2 μm. In (I) the low efficiency of composite particles in initiating crazes was attributed to two separate causes. In one case where the composite particles had the KRO-1 Resin morphology where the majority phase was a topologically continuous stiff phase of PS, the particles were too stiff to result in enough local stress concentration

* Department of Mechanical Engineering.
† Department of Chemical Engineering.

0032-3861/85/040529-14$03.00

to initiate crazes[13], even though their size was well above 1–2 μm. In the other case where the particle morphology consisted of concentric spherical shells of PB and PS, each with a thickness of about 20–40 nm, the particle size was too small ($\sim$0.4 μm) even though the particles were sufficiently compliant to initiate crazes[13]. Thus, the results of (I) pointed in the direction of a need to increase the compliance of composite particles at a size larger than 1–2 μm.

An attractive technique of changing the morphology and properties of composite particles is by blending additional low molecular weight homopolymer components into the already composite particles. As has been demonstrated by Kawai and coworkers[14,15], low molecular weight homopolymer components are solubilized by the individual block components in block copolymers and are therefore an effecive means for fine-tuning existing morphologies or even initiating morphological transformations. That such procedure is effective in improving toughness in rubber modified heterogeneous polymers has already been demonstrated by Kruse[16] who has obtained striking improvements in the toughness of certain HIPS and ABS systems by blending into them additional low molecular weight PB. The limit to which low molecular weight homopolymer can be solubilized in existing block copolymers is governed by the respective molecular weights of the coarsening agent, the particular block copolymer, and its starting morphology. This subject has been considered recently in some detail by Leibler[17].

Here we will report the results of such an investigation on morphological modification of composite particles by blending of low molecular weight homopolymers into the commercial K-Resin paticles in high molecular weight PS matrices. The study will demonstrate the vital importance of the particle morphology in governing its stiffness, and the rubber content in governing its overall thermal expansion, since both the stiffness misfit and the thermal expansion misfit play equally important roles in initiating crazes around particles under stress.

EXPERIMENTAL PROCEDURES

Materials and microstructures

The same commercial block copolymers used in (I), i.e., the Phillips KRO-1 and KRO-3 Resins were used in this study as the basic building blocks of composite particles in matrices of the same high molecular weight PS, i.e., Lustrex HH-101. In this paper we shall report the results on the modification of the KRO-1 blends only.

The physical and mechanical properties of K-Resins have been listed in Table 1 of (I) together with the corresponding properties of the Lustrex HH-101 PS making up the majority phase. Routine n.m.r. measurements show that PB in predominantly 1,4 addition makes up about 23% of the weight of KRO-1[18]. Measurements by DTA-TMA show two distinct transitions near -90°C and 95°C for KRO-1, corresponding to PB and PS respectively and indicating that for the purposes of mechanical modelling, the pure block copolymer acts as a two-phase mixture of PB and PS. The equilibrium morphology of KRO-1 Resin, shown in Figure 1 of (I), is in the form of randomly wavy and often interconnected rods of PB of an average diameter of 20 nm, surrounded by a topologically continuous block phase of PS. The majority phase of HH-101 PS used to form the matrix in both (I) and in this study is used commercially for biaxially oriented film and for foam sheet extrusions. It has been kindly furnished by the Monsanto Polymer Products Company of Springfield, Massachusetts. It contains no additives outside a molecularly dissolved tinting agent of undisclosed nature at a composition of 0.16% by weight.

A series of low molecular weight PS and PB were used as coarsening agents, each having a narrow molecular weight distribution with polydispersity indices of around 1.1. These coarsening agents included PS with a molecular weight of 64 kg mol^{-1} designated as PS64K, and PB with molecular weights of 3, 22 and 44 kg mol^{-1} designated as PB3K, PB22K and PB44K, respectively. The PB22K, PB44K and PS64K were prepared locally by anionic polymerization. Proton n.m.r. spectroscopy has shown that the PB are predominantly (87%) 1,4 addition. The PB3K was purchased from Polyscience, Inc. of Warrington, Pennsylvania. This too was found to be in predominantly 1,4 addition.

Different blending trials with these homopolymers were necessary because the multiplicity of the arms in the star-shaped nature of KRO-1 molecule has not been disclosed. Successful solubilization of additional homopolymer into the block copolymer morphology, on the other hand, requires that the molecular weight of the homopolymer additive be less than that of the unknown molecular weight of the branch arm of the star molecule.

Film preparation

The procedures used for film preparation by centrifugal solvent casting, employing special schedules for solvent evaporation and annealing were described in detail in (I) and will not be repeated here. The resulting films were of high quality, translucent, having smooth surfaces and constant thickness. The thickness from batch to batch, however, varied in the range of 0.6–0.7 mm.

Microscopy and tensile testing

The details for light microscopy and transmission electron microscopy, as well as those for tensile testing, were also described in (I). All tensile testing was performed at room temperature and at an average strain rate of 1.3×10^{-4} s^{-1}.

EXPERIMENTAL RESULTS

Blending with PS64K

The morphological wave length of KRO-1 Resin is governed principally by the molecular weights of the block components of PB and PS. The overall weight average molecular weight of KRO-1 is 179 kg mol^{-1}[18]. For a 0.23 weight fraction of PB, this established weight average molecular weights for the PS and PB components of 137.8 and 41.2 kg mol^{-1} respectively. Thus, if the average [*] star-shaped KRO-1 molecule had n arms, the relevant molecular weight of any individual arm would be $137.8/n$ for PS and $41.2/n$ for the PB blocks. Consequently, a narrow molecular weight coarsening agent of PS64K could serve as a molecular 'solvent' for $n=2$, but not for $n=3$.

* Gel permeation chromatography shows that both KRO-1 and KRO-3 Resins are blends of several separate block copolymers with different individual molecular weights.

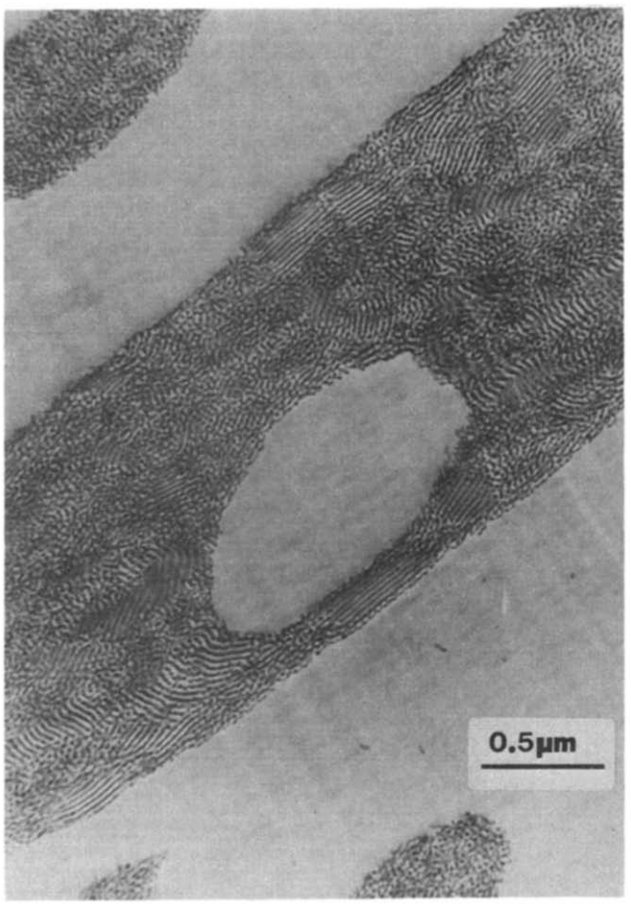

Figure 1 Interior of composite particle resulting from an attempt to blend additional PS64K into the KRO-1. The additional PS64K is inside the particle but has not been solubilized into the KRO-1 morphology

In the blending trial with PS64K, a weight ratio of 0.5 was chosen for PS64K/KRO-1, maintaining, however, an overall composite particle volume fraction of 0.217 in the HH-101 matrix.

The TEM micrograph of *Figure 1* shows that the added PS64K enters the particles, but that it is not solubilized into the PS block component. It has merely associated with the KRO-1 particle which has an unaltered morphology. Areal image analysis of micrographs has established that the majority of the added PS64K is indeed associated with the KRO-1 particles and that only a small fraction has been solubilized into the matrix HH-101 PS. We conclude from this trial that $n>2$. *Figure 2* shows the stress–strain curves of four such blends. Comparison of these curves with Figure 7 of (I) indicates a performance almost indistinguishable from the unmodified KRO-1 blends in HH-101 PS. Both results show a high overall modulus and craze yield stress in the vicinity of 28 MPa, and a plastic strain to fracture of around 0.04. This rather unattractive result is not surprising since the added PS64K of a high modulus has not been incorporated into the PS of the block, but has merely increased the average stiffness of the already very stiff composite particle. Had it been solubilized into the PS block phase of the KRO-1 morphology, the increase in the PS wave length would have been only 10%—far too small to influence the range of the concentration of stress at the periphery of the particle resulting from the internal morphology.

Blending with PB44K, PB22K and PB3K

On the basis of the negative results on solubilization of the PS64K homopolymer into the KRO-1 Resin microstructure, it is clear that $n>2$ for PS which is likely to be true also for the PB arms of the KRO-1 molecule. Therefore, a successful solubilization trial will require a molecular weight for the additional PB homopolymer less than 20.8 kg mol^{-1}. That this was indeed the case is verified by the negative results of the blending trials utilizing PB44K and PB22K. In these trials, also, the overall composite particle volume fraction was maintained constant at 0.217 and the same ratio of 0.5 of low molecular weight homopolymer to KRO-1 Resin was used in the blends. The free surface of the cast films pointing toward the centre of the spin cup was found to contain a sticky layer that was identified to be largely the centrifugally separated low molecular weight PB homopolymers. The cast films were found to be very fragile, having little mechanical integrity. *Figures 3a* and *3b* show two TEM micrographs of these blends which indicate that the low molecular weight PB coarsening agents have associated themselves primarily with the KRO-1 particles, but as in the case of the PS64K results, they too have failed to be solubilized into the KRO-1 morphology. Large spherical droplets of the PB44K and PB22K are visible inside the composite particles of KRO-1 Resin whose morphology has remained unaltered in form as well as in scale.

The blending trials with PB3K in contrast have produced dramatically different results. In these trials, the overall volume fraction of particles was again kept constant at 0.217 to make the results directly comparable to the results of the previous investigations. In these trials, however, a wider range of weight ratios of PB3K/KRO-1 was investigated, including 0.125, 0.250, 0.333, 0.500, 0.750 and 1.000. The computed compositional details for these blends are summarized in *Table 1*. *Figure 4* shows these compositional trends as a function of the PB3K/KRO-1 ratio employed.

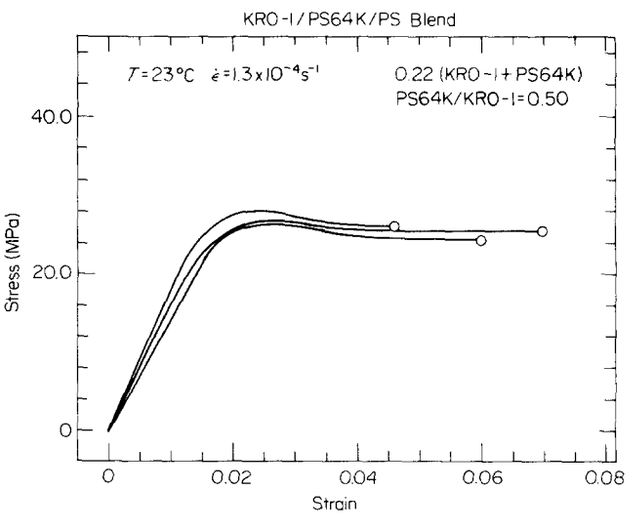

Figure 2 Stress–strain curves of KRO-1/PS blends modified with PS64K at a blend ratio of PS64K/KRO-1 = 0.5. Tested at room temperature at a strain rate of 10^{-4} s^{-1}

Transmission electron microscopy of the structure of the cast films has verified that the initial additions of PB3K are completely solubilized into the KRO-1 particles. The micrographs show that even for the smallest ratio of PB3K/KRO-1 of 0.125 a morphological transformation is initiated from the typical KRO-1 wavy rod morphology to a parallel lamellae morphology. *Figure 5a* shows this transformation inside composite particles. While large particles show a new morphology consisting of parallel layers of PS and PB, small particles retain the characteristic KRO-1 morphology of randomly wavy and interconnected rods. The transformation indicates that the KRO-1 morphology with a weight fraction of 0.23 PB exists very close to the border of a region of phase transformation, and that the addition of PB3K accomplishes the transformation in a certain fraction of the KRO-1. As the PB3K/KRO-1 ratio is increased the transformation becomes more complete. As *Figure 5b* shows, for a ratio of 0.250 of components the particles are now almost completely made up of the concentric spherical shell morphology of PB and PS layers. There are, however, some small particles that still retain the KRO-1 morphology. *Figure 5c* shows the morphology of the PB3K/KRO-1 = 0.333 blend. In this case the morphological transformation is closer to completion.

When the PB3K/KRO-1 ratio becomes 0.50, some of the large particles with the concentric spherical shell morphology show again a separate dark phase that can only be PB3K that now is apparently at a volume fraction beyond the solubility limit of this homopolymer in the KRO-1 microstructure. *Figure 5d* shows several examples of such ill-defined black regions with jagged borders inside some large composite particles. The jagged borders suggest a very low level of interface energy between the excess PB3K and the spherical shell morphology. The

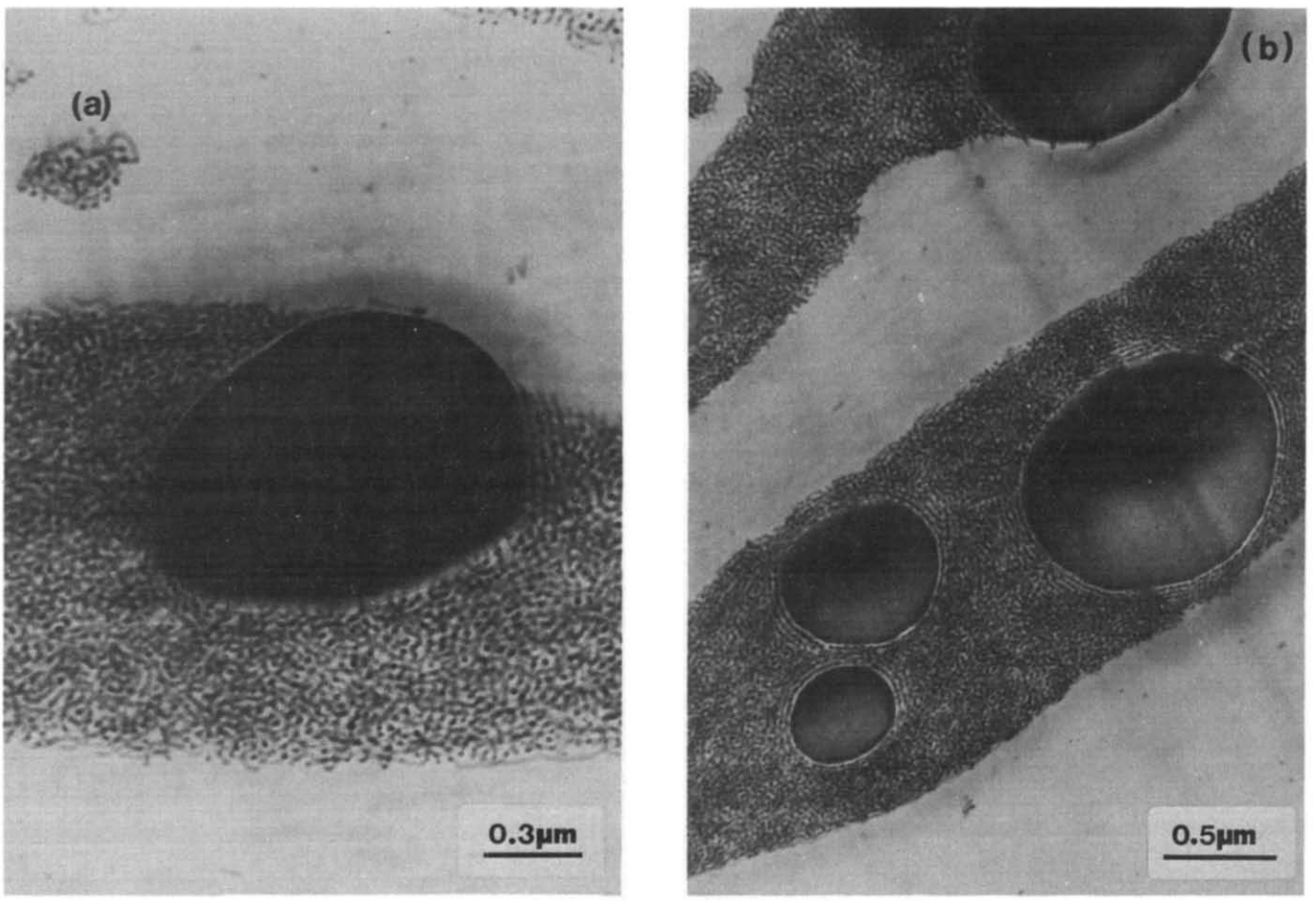

Figure 3 Interiors of composite particles resulting from attempts to blend additional PB into them: (a) PB44K addition; (b) PB22K addition, both at blend ratios of PBXXK/KRO-1 = 0.5. Clearly the PBXXK has not been solubilized into the KRO-1 morphology

Table 1 Compositional details of PB3K blends into KRO–1/HH–101 PS heterogeneous polymers

PB3K/KRO–1 Weight ratio	Wt. fraction PB3K	Wt. fraction PB of KRO–1	Wt. fraction total PB
0	–	0.050	0.050
0.125	0.024	0.044	0.068
0.250	0.043	0.040	0.083
0.333	0.054	0.037	0.092
0.500	0.072	0.033	0.105
0.750	0.094	0.028	0.122
1.000	0.108	0.025	0.133

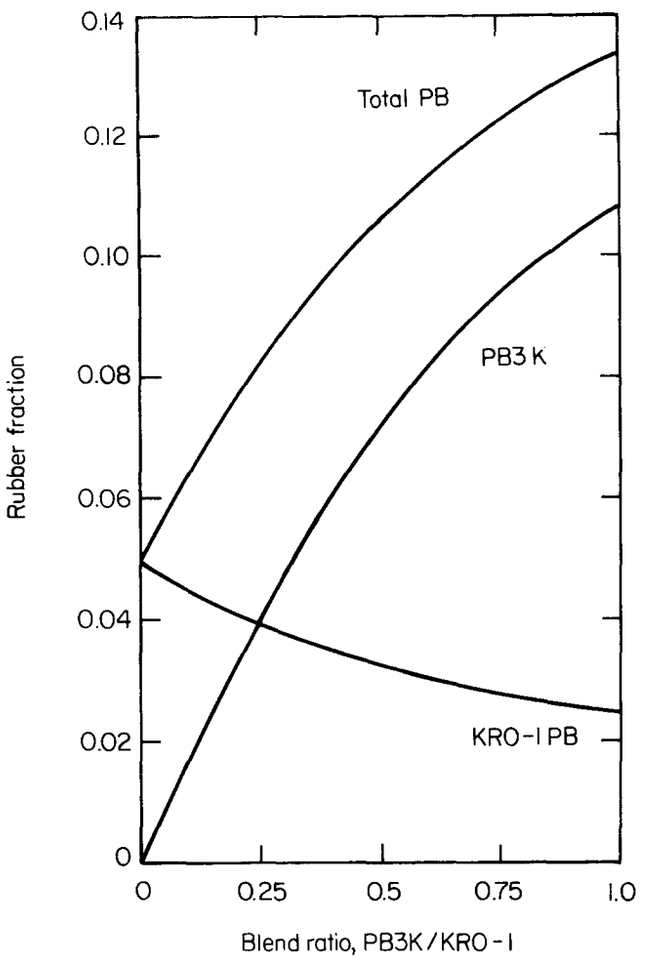

Figure 4 Changes in fraction of total PB, low molecular weight PB, and PB of KRO-1 in composite particles as a result of blending additional PB3K into them

trend of decomposition of the lamellar phase and the excess PB3K continues for further increases in the PB3K/KRO-1 ratio to 0.750 and 1.000, as *Figure 5e* and *Figure 5f* show for these two blend ratios. Examination of the morphology of the large particle in *Figure 5f* for the case of PB3K/KRO-1 = 1.000 shows now a reversion of the particle morphology back to that of pure KRO-1 coexisting with the PB3K component. *Figure 6* for the PB3K/KRO-1 = 0.750 composition shows that this reversion is gradual, where the particle in this micrograph shows the coexistence within one particle of three separate morphologies: the KRO-1 morphology, the alternating lamellae morphology resulting from the solubilization of some PB3K into the PB block domains of the KRO-1, and finally an excess of PB3K that is separated from the other two phases by jagged interfaces with apparently quite low energy. The explanation of this morphological reversion is not clear.

Since the additional PB3K is expected to be incorporated into the PB domains of the KRO-1 morphology, a change in domain thickness with additional PB3K solubilization should be expected. Thus, as *Table 1* shows, if the entire amount of PB3K were absorbed into the PB of KRO-1, the thickness of the PB domains should increase by a factor of 2.66 as the PB3K/KRO-1 ratio increases from 0–1.00. The effective measurable thickening, however, should be much less. This is because addition of PB3K in the range of ratios 0–0.25 accomplishes the morphological transformation which, until it becomes complete at about 0.33, is at constant structure of the lamellar phase as the two coexisting morphologies gradually displace each other. On the other hand, the solubility limit of PB3K appears to be reached at a PB3K/KRO-1 ratio of 0.50, beyond which a decomposition is observed with an excess PB3K phase being rejected. Hence, the thickening of the PB lamellae is likely to be only in the range (of the PB3K/KRO-1 ratio) of 0.3–0.5 resulting in a measurable thickening of only by a factor of 1.33. The actual measurements in the range of the blend ratio of 0.3–0.5 show no detectable amount of lamellar thickening beyond the background scatter resulting from the variations due to sectioning at different distances of particles between their equators and poles, and the normal thickness variations that should be present due to the different curvature stresses among domains of widely different particle sizes.

Stress–strain response of PB3K modified blends

Figures 7 of (I) and *Figure 2* of this study indicate that the flow stress of the KRO-1/HH-101 blends with composite particles having the KRO-1 morphology is above 28 MPa in the range of the craze yield stress of unmodified PS, and that the strains to fracture at this level of the flow stress are less than about 0.04. The addition of PB3K in the ratio of 0.125 to KRO-1 results in the initiation of a morphological transformation in at least some of the particles with an accompanying dramatic drop of the craze yield stress of 11.5–13 MPa and an increase in the plastic strain to fracture to between 0.26–0.34 as is shown in *Figure 7a*. The curves show a typical yield phenomenon giving the levels for initiation of the required volume density of active craze front that gives a match between the imposed machine rate and the cavitational strain rate due to craze matter conversion[18]. Once the process is initiated the advance of a constant volume density of active craze front at steady state is possible at a lower flow stress of about 8 MPa in this case. The curves, however, show that at the straining continues the low level of flow stress increases in several steps until finally fracture occurs. This increase is attributed to the final exhaustion of composite particles that have undergone the morphological transformation, and were acting as the most compliant and effective sources of craze initiation. *Figure 7b* shows the stress–strain response of the blends with the PB3K/KRO-1 ratio of 0.25. The upper yield stress necessary to initiate the required active craze front has decreased now to a range of 10–10.5 MPa, while the flow stress has dropped to about 8.5 MPa, accompanied by a rise in the strain to fracture between 0.3–0.48. These advantageous changes have become possible due to the much more complete conversion of the composite particles to the high compliance morphology of concentric spherical shells. *Figures 7c* and *7d* show the continuing trend of improving behaviour for increasing PB3K/KRO-1 ratios of 0.333 and 0.50. For these two blend ratios there is little additional decrease in the upper yield stress which remains at around 10 MPa, but a small additional decrease of the plateau flow stress to about 8 MPa. The strain to fracture, however, continues to increase to about 0.80 in the case of one of the 0.50 blends. In this latter case, also, there is no perceptible rise in flow stress toward the end of the experiment indicating no visible exhaustion of compliant particles that govern the perpetuation of the

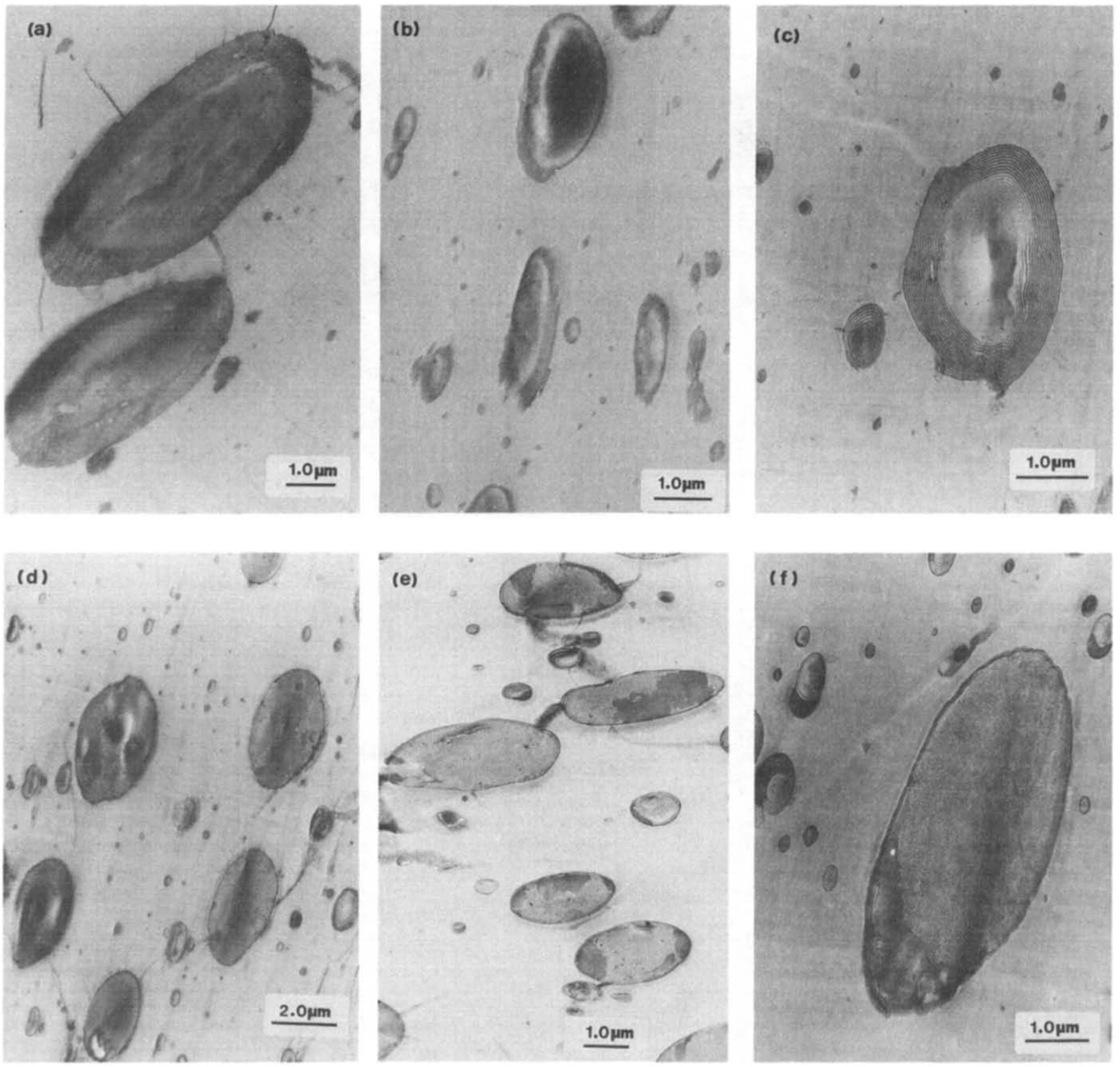

Figure 5 TEM micrographs with increasing blend ratio of PB3K/KRO-1: (a) blend ratio of 0.125, composite particles with two coexisting internal morphologies of randomly wavy rods and concentric shells; (b) blend ratio of 0.25, particles with a large fraction of spherical shell morphology; (c) blend ratio of 0.33, most particles have a nearly perfect spherical shell morphology; (d) blend ratio of 0.50, spherical shell particles with some free PB3K beginning to re-precipitate; (e) blend ratio of 0.75, substantial volume fraction of PB3K has precipitated out; (f) blend ratio of 1.00, particles with re-precipitated free PB3K and KRO-1

active craze front per unit volume necessary to match the specimen extension rate to that imposed by the machine. Some variation in the fracture strain is found, however, in all cases.

When the PB3K/KRO-1 ratio increases beyond 0.50 for which the TEM study had shown a separation of PB3K phase inside the particle, both upper yield stress as well as the plateau flow stress continues to drop while now the strain to fracture also sharply decreases as is shown in *Figure 7e* and *7f* for the blend ratios of 0.75 and 1.0. As the particles incorporate more and more rejected PB3K phase with internally liquid-like behaviour, more particles begin to come apart under the level of the plateau stress and initiate local fracture. At the blend ratio of 1.0, the material has lost almost all of its attractive toughness.

The trend of behaviour with increasing PB3K/KRO-1 ratio is summarized in *Figure 8a* and *8b*, showing the reduction of the upper yield stress and the accompanying rise and fall of the strain to fracture. In *Figure 8a* the very large decrease in upper yield stress with increasing PB3K/KRO-1 ratio is due to the morphological transformation that provides at least some particles with sharply increased compliance to initiate crazes under much lower stress due to the significantly increased concentration of effective stress and negative pressure at the particle periphery. The dotted back-extrapolated curve would give the craze yield stress of a blend ratio of zero, but with a concentric spherical shell morphology rather than the randomly wavy rod morphology actually observed at this compositon[8].

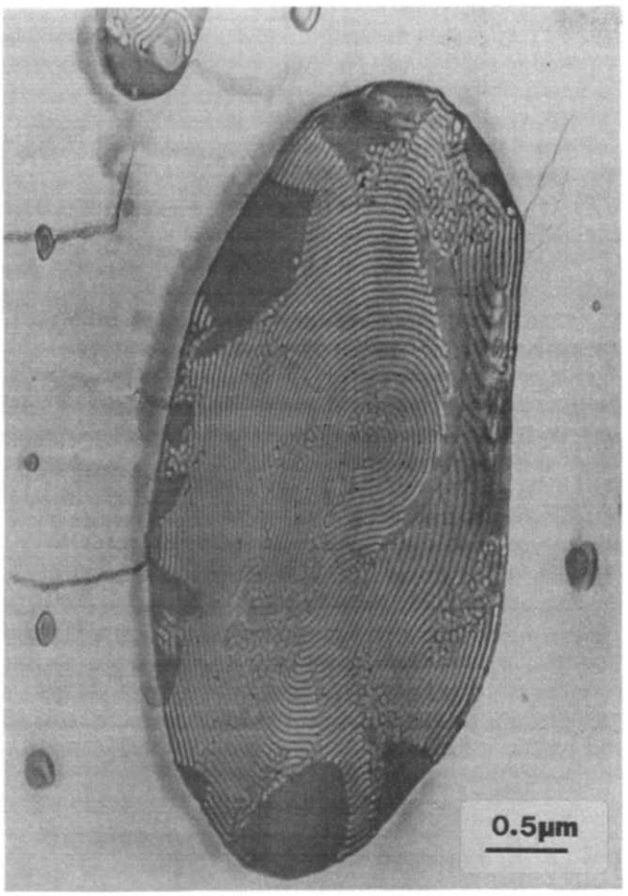

Figure 6 TEM micrograph of particle in a blend of PB3K/KRO-1 of 0.75 showing the coexistence of three morphologies

Blends with other particle fractions

To determine the effect of the volume fraction of composite particles at constant morphology, a blend was prepared in which the PB3K/KRO-1 ratio was kept at the most advantageous level of 0.50, and the volume fraction of the particulate phase was changed from 0.217 down to 0.15. In this manner the total rubber weight fraction in both the KRO-1 and the additional PB3K was decreased down to 0.073. On the basis of the results of (I), a small decrease in the average particle size is expected while the total number density of particles remains constant. The stress–strain response to the blend is shown in *Figure 9*, which should be compared with the results in *Figure 7d*. A small rise in both the upper yield stress (from 10.2 to 11 MPa) and the plateau flow stress (from 8 to 8.6 MPa) is observable, which in all probability is due to the decrease in the average particle size and the attendant reduction in the volume density of the particles with requisite size for craze initiation with the appropriate high compliance. Also seen, however, is a reduction in the strain to fracture to within 0.3–0.5 and several step increases in the plateau flow stress indicating the exhaustion of the most compliant particles that are effective craze initiators.

Morphological features of crazes

Because of the opacity of the partially crazed (PB3K)–(KRO-1) PS blends, TEM was widely used to study craze morphology and craze distribution in the deformed and fractured specimens.

The blending modification with PB3K produces sharp increases in craze density with increasing PB3K/KRO-1 ratio. The TEM micrographs show that craze development depends strongly on particle structure. For the blends with PB3K/KRO-1 ratio of around 0.125 the crazes that have formed are usually short and thin as those shown in *Figure 10a*. The Figure shows that large particles are the preferred sites for craze initiation. As the PB3K/KRO-1 ratio is increased the number of crazes around particles as well as their length increases as is shown in *Figure 10b* for the blend ratio of 0.250. Large particles are still the ones that initiate most crazes, but the craze initiating effectiveness is seen to gradually extend downward also to somewhat smaller particles. Examination of additional micrographs has disclosed that the majority of crazes are initiated at particles that have a higher degree of structural coherence. When the PB3K/KRO-1 ratio reaches 0.50, the density of crazes in the samples extended to fracture becomes very high. These crazes are seen to branch, interact and create a complex pattern. *Figure 10c* shows a typical region of an extensively crazed sample showing nearly complete coverage of particle peripheries with emanating crazes. In the 0.5 blend ratio where craze initiating efficiency of particles has reached a peak, this effectiveness has also extended down to considerably smaller particles that would usually be considered outside the range of nucleation. *Figure 11* shows several sub-micron particles, such as the ones identified as A, which seem to be unambiguously the sites for craze initiation.

When the PB3K/KRO-1 blend ratio exceeds 0.5 and phase decomposition occurs inside the particles with separation of a PB3K component, crazing around large particles becomes increasingly associated in micrographs with tears inside the particles. This is shown in *Figure 12* for a sample with a blend ratio of 0.750. While clearly some of this tearing can be a microtoming artifact, similar tears have not been found in micrographs of other blend ratios or those that have been prepared from uncrazed samples. Therefore, these tears are interpreted to be the principal internal sites of fracture initiation. Samples with a blend ratio of 1.0 have been found to be so fragile that it has not been possible to microtome them.

Stereology of crazes and craze distribution

The analysis of craze microstructures in the electron micrographs for the specimens stretched to the vicinity of their fracture strains reveals a great deal of information essential to the understanding of the role of the PB3K modifier of the KRO-1 particles. The crazes around as many as 1500 particles were counted, and an overall craze density was determined. *Figure 13a* shows these results on craze density graphically. The error bars account for the variability due to non-uniform distribution of particles. The unmodified blend of KRO-1 and PS studied in (I) yields a craze density of 10^7 distinguishable craze planes per cm^2, developed at relatively high stresses. As discussed in (I), craze initiation in the unmodified blends is limited to surfaces, while particles are not important sites of craze initiation. With the addition of PB3K, the craze yield stress drops sharply. The blend with the PB3K/KRO-1 ratio of 0.125 shows a number density of crazes comparable to that of the unmodified blend. But the micrographs of the PB3K modified blends clearly show that crazing is initiated by the particles at low stresses. Furthermore,

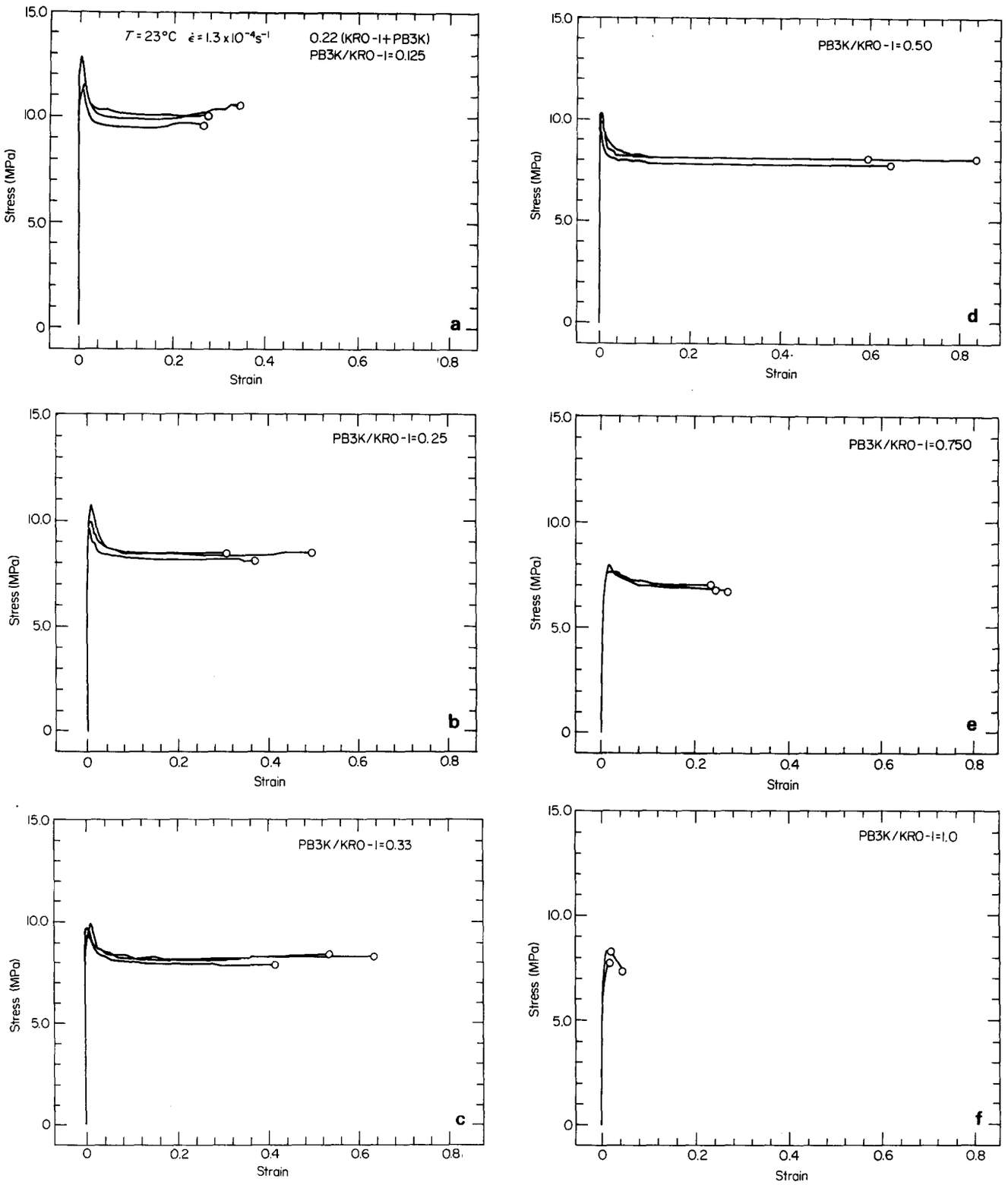

Figure 7 Stress–strain curves of modified blends, all with a particle volume fraction of $c_p = 0.217$: (a) blend ratio of 0.125; (b) blend ratio 0.25; (c) blend ratio 0.33; (d) blend ratio 0.50; (e) blend ratio 0.75; (f) blend ratio 1.00

both the lengths and the thicknesses of crazes are larger in the PB3K modified blend with a blend ratio of 0.125 in comparison with the crazes in the unmodified blends. This results in a substantial increase in the strain-to-fracture in the former over the latter. Another distinguishing feature between these two cases having the same number density of crazes is that in the modified blend the plateau flow stress is much lower, resulting in a less severe loading condition of the already formed craze matter.

The dependence of craze density on the PB3K/KRO-1 ratio between 0–0.5 follows qualitatively that of the plastic strain-to-fracture. Although the addition of small quantities of PB3K leads to a sharp drop in craze yield stress with profuse craze initiation, the value of plastic strain-to-

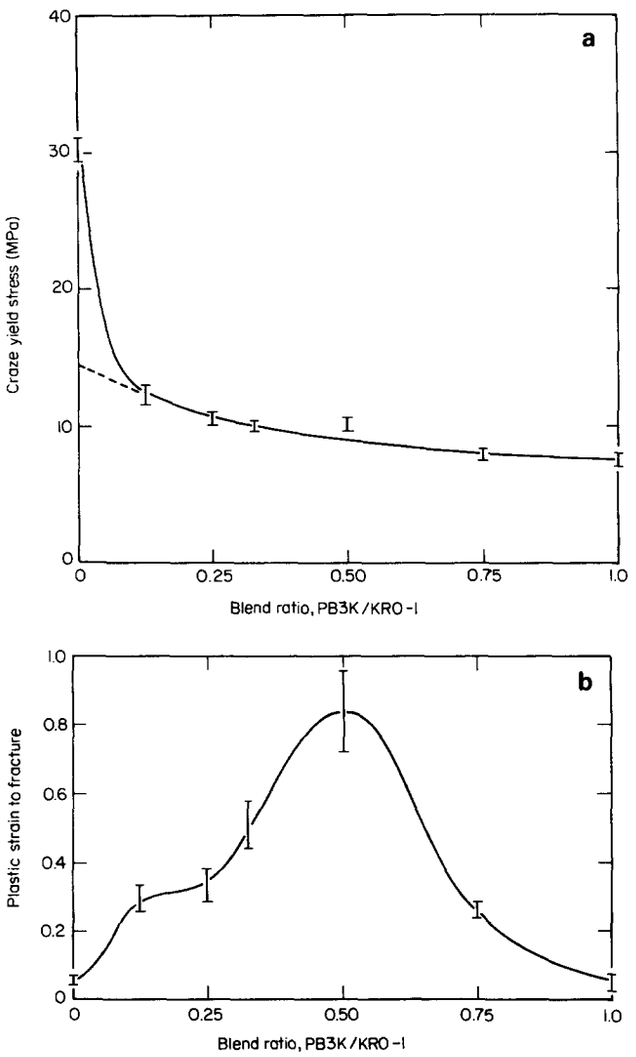

Figure 8 Effect of the increasing particle blend ratio on mechanical properties: (a) craze yield stress; (b) plastic strain-to-fracture

fracture is strongly dependent on the ability of the particles to sustain such low stresses. *Figure 13b* gives the average number of crazes per particle in the respective blends at the fracture strain. For the blend ratio of 0.125 the Figure gives that the number of crazes per particle is only 0.2. This average number of crazes per particle increases rapidly with increasing PB3K/KRO-1 blend ratio, and for a ratio of 0.5 reaches a level as high as 0.9. *Figure 13b* furnishes another graphic evidence for the high craze initiating efficiency of large particles. The frequency distribution of the craze initiating efficiency of particles of different sizes is demonstrated dramatically in *Figures 14a–e*, showing this information for all the five blend ratios that were studied. Clearly as the blend ratio increases and the particle compliance rises, the craze initiating efficiency of a particle of given size increases. In addition, the size of the threshold particle that is just able

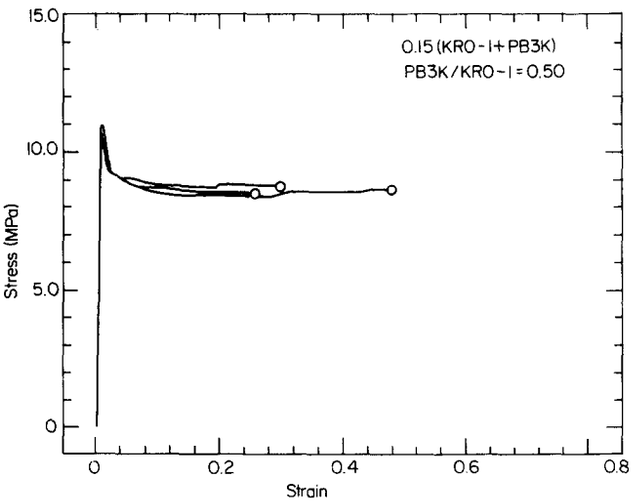

Figure 9 Stress–strain curves of a modified blend with a particle blend ratio PB3K/KRO-1 of 0.5, at a particle volume fraction $c_P=0.15$

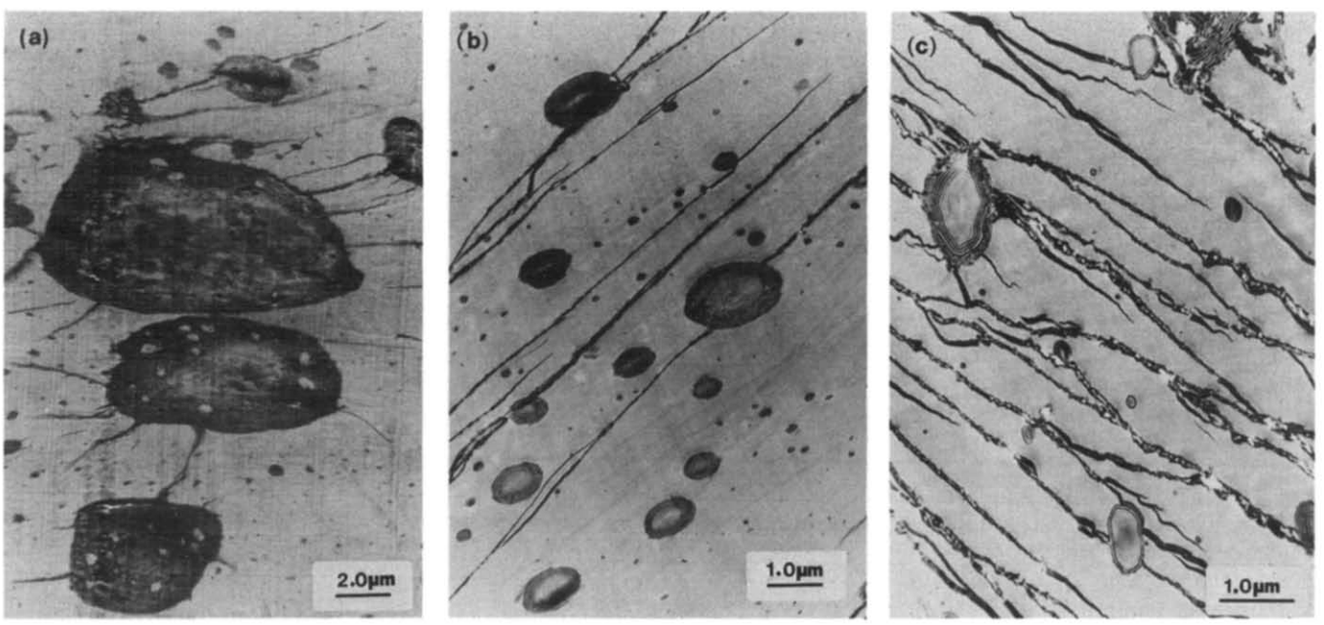

Figure 10 TEM micrographs of crazes in PB3K/KRO-1 blends at the fracture strain: (a) blend ratio of 0.125; (b) blend ratio of 0.25; (c) blend ratio of 0.5

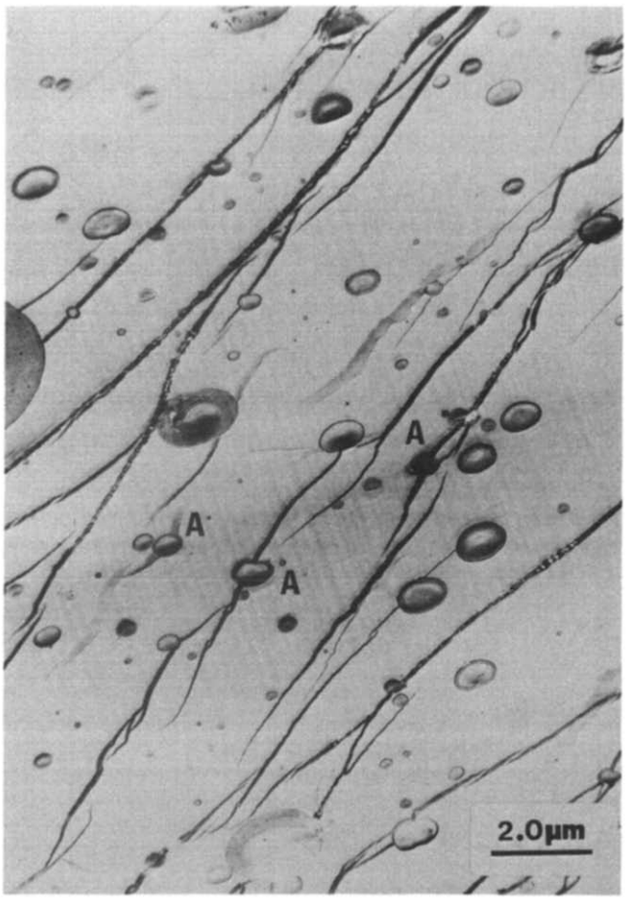

Figure 11 TEM micrographs of craze initiation from well-formed small spherical shell particles (A) in a blend with PB3K/KRO-1 ratio of 0.5 in the particles

to initiate crazes becomes progressively smaller. This trend peaks for the blend ratio of 0.5 and begins to decline again as the PB3K precipitation begins inside the particles, when the blend ratio exceeds this value. As *Figures 5e* and *5f* show, the particle morphology becomes irregularly heterogeneous and the stiff KRO-1 morphology inside the particles reappears. With the relatively large fraction of free PB3K existing inside the particles, however, the overall stiffness of the particles remains low, as *Figure 15a* establishes. Thus, the apparent decline in craze initiation effectiveness is in all probability due to the progressively earlier onset of fracture from the internal cavitation or interfacial separation of the large composite particles, which cut short the craze plasticity process.

Examination of the micrographs of craze morphology shows that particle-structure-controlled properties govern the average craze thickness at the particle periphery that is covered with emanating crazes. *Figure 15a* shows a measure of this effect, in a plot of the average ratio of craze thickness to the nearest particle spacing. The Figure shows that this ratio first decreases and then increases. Since, as is shown in *Figure 13b*, the number of crazes per particle monotonically increases with blend ratio until this ratio becomes 0.5, the initial decrease in average craze thickness with increasing blend ratio may signify an increasing craze nucleation efficiency but a slight difficulty in craze thickening. Thus, the tendency shown in *Figure 15a* is not altered when the phenomenon is plotted as the product of *Figure 13b* and *Figure 15a*, which gives the total craze thickness per particle (per mean particle spacing), shown also in *Figure 15b* by the open circles. The trend shown in *Figures 15a* and *15b* indicates that the compliance of the particle continues to increase with increasing blend ratio even though the morphology of the particle becomes irregular and PB3K precipitates out beyond a blend ratio of 0.5.

DISCUSSION

Mechanical properties of composite particles

Clearly the results of our previous study (I) as well as the results of our PB3K blending experiments reported here point toward the key importance of the changing mechanical properties of the composite particles with blending. Once the particles are sufficiently large so that craze initiation is no longer impeded by an insufficiency of size of the local highly stressed volume, multi-axial craze initiation criteria developed for application in bulk should be applicable locally around the particles, as was attempted by Oxborough and Bowden[11,12]. For this purpose the mechanical properties of the composite particles need to be known with some accuracy. Once the morphology of the particle is established, the elastic and other physical properties of the particles are calculable by resorting to the developments of composite theory and other numerical modelling techniques employing, e.g., finite element approaches.

It is usual to consider as a first approximation the

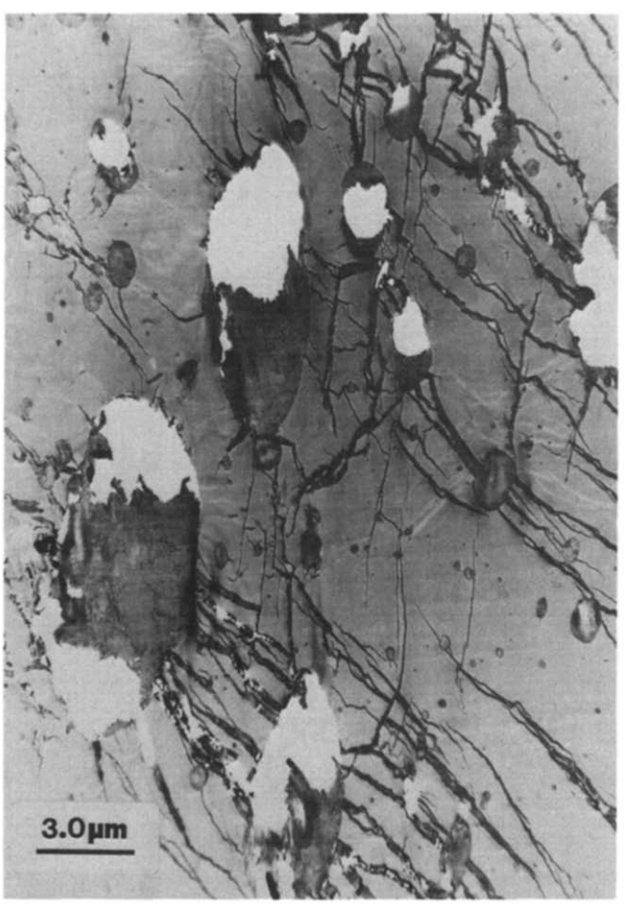

Figure 12 TEM micrograph showing tear origins inside particles with reprecipitated free PB3K components in a blend with PB3K/KRO-1 ratio of 0.75 in the particles

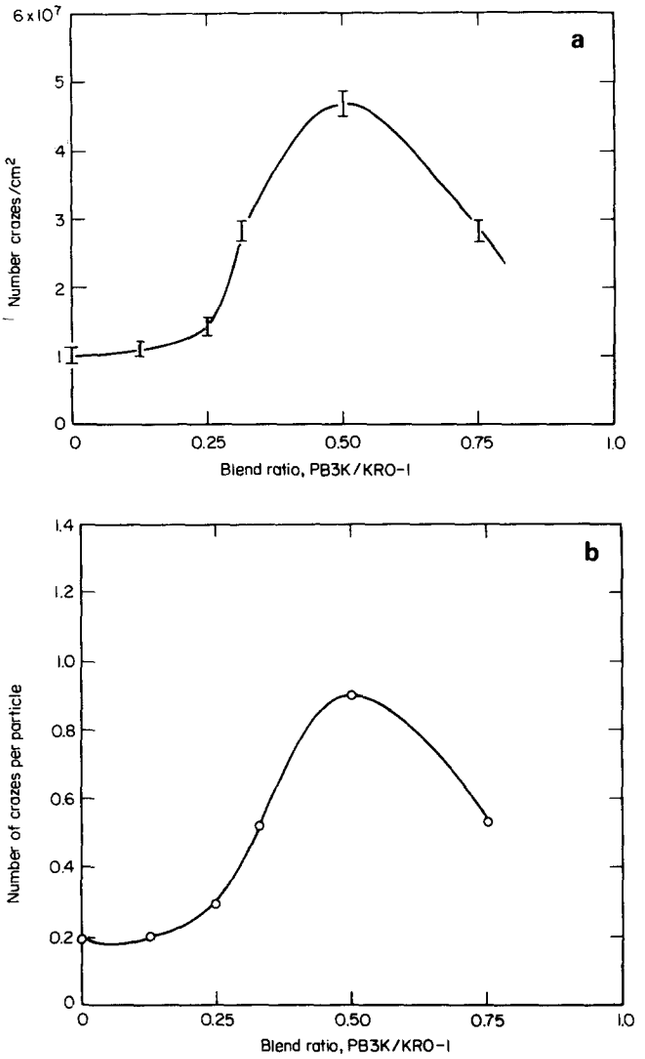

Figure 13 Increasing craze initiating effectiveness of composite particles with increasing PB3K/KRO-1 blend ratio: (a) number of separate crazes/cm^2 in micrographs; (b) number of crazes emanating per particle

microstructure of a composite particle to be smoothed out and replaced with averaged elastic and thermal properties. Although this approach is acceptable for the typical unmodified KRO-1 particles discussed in (I), as well as the usual HIPS particles, the smoothing is clearly inappropriate for the spherical shell particles shown in *Figure 5c*. Such more specific modelling of particles with spherical shell morphology in comparison with particles of some other morphologies, has been done by Boyce *et al.*[13] and will be reported elsewhere. Here we will make use of their results.

The KRO-1 particle

The behaviour of the KRO-1 particles with randomly wavy rod morphology in the presence of a surrounding that is also occupied by a given volume fraction of similar particles is calculable by a combination of approaches which in general also apply to the spherical shell particles.

First, the stresses produced by the thermal expansion misfit between the particles and their surroundings constitutes a problem of spherical symmetry where the effect of the surrounding particles is taken into account by solving this thermal misfit problem as one of two concentric spheres in which the centre sphere represents the volume fraction of the particulate phase and the outer shell the matrix allocated to one generic particle. The average moduli and the average coefficient of expansion of the particles are obtained first from the moduli and coefficients of thermal expansion of PB and PS by

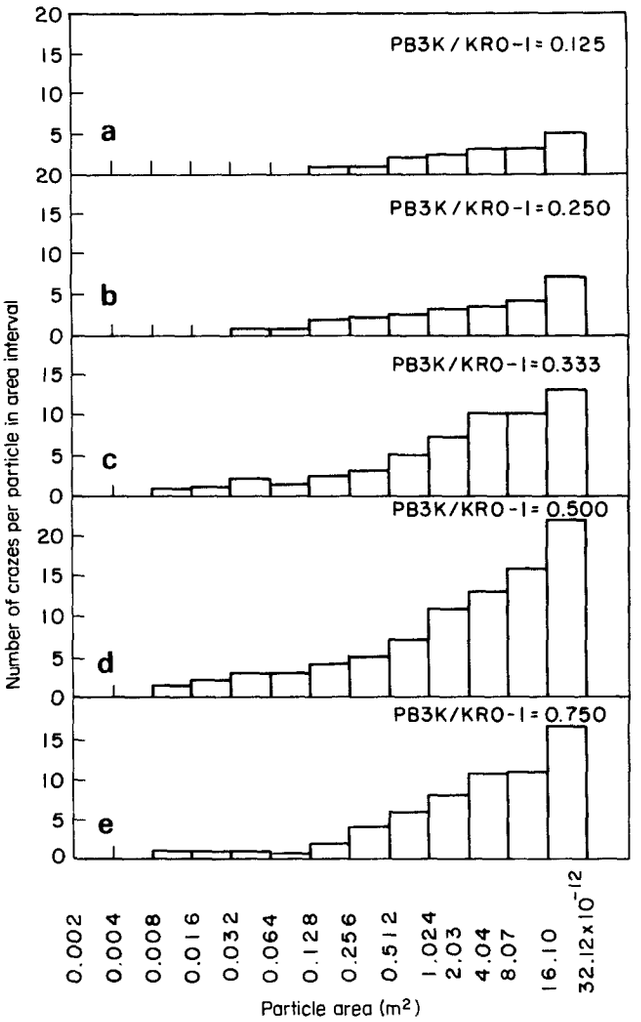

Figure 14 Histogram of number of crazes per particle in a given interval of particle cross-sectional area at fracture for five particle blend ratios PB3K/KRO-1: (a) 0.125; (b) 0.250; (c) 0.33; (d) 0.50; (e) 0.75

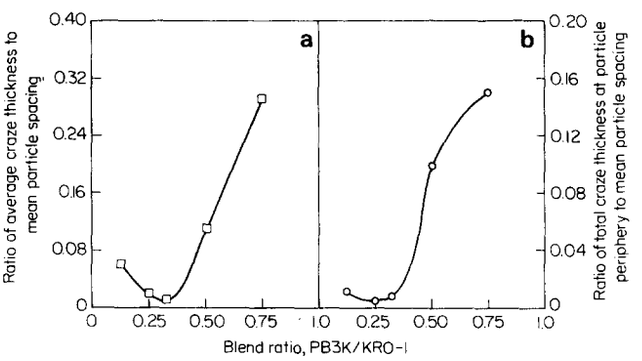

Figure 15 Changing ratio of: (a) average craze thickness to mean particle spacing; (b) total craze thickness at particle periphery to mean particle spacing, with increasing blend ratio PB3K/KRO-1

considering that the PS in the morphology of the particle is topologically continuous permitting the use of Chow's method[19,20]. The result of this computation gives the following average Young's modulus E_P, bulk modulus K_P and Poisson's ratio ν_P:

$$\frac{E_P}{E_{PS}}=\left[1+\frac{c_{PB}\left(\frac{K_{PB}}{K_{PS}}-1\right)}{3+(1-c_{PB})\left(\frac{1+\nu}{1-\nu}\right)\left(\frac{K_{PB}}{K_{PS}}-1\right)}-\frac{2}{3-(1-c_{PB})\frac{2(4-5\nu)}{5(1-\nu)}}\right] \quad (1)$$

$$\frac{K_P}{K_{PS}}=\left[1+\frac{c_{PB}\left(\frac{K_{PB}}{K_{PS}}-1\right)}{1+\left(\frac{K_{PB}}{K_{PS}}-1\right)(1-c_{PB})\frac{1+\nu}{3(1-\nu)}}\right] \quad (2)$$

$$\nu_P=\left(1-\frac{E_P}{3K_P}\right)\Big/2 \quad (3)$$

where properties with subscripts PB and PS refer to those of PB and PS respectively, where ν is the Poisson's ratio of PS, and where in the computation of the Young's modulus of the particle, the shear modulus of PB was considered to be negligibly small in comparison with the shear modulus of PS. The corresponding computation for the average volumetric coefficient of thermal expansion of the particle γ_P gives:

$$\gamma_P=\left[\gamma_{PS}+\frac{c_{PB}\left(\frac{K_{PB}}{K_{PS}}\right)(\gamma_{PB}-\gamma_{PS})}{1+\left(\frac{K_{PB}}{K_{PS}}-1\right)\left[(1-c_{PB})\frac{1+\nu}{3(1-\nu)}+c_{PB}\right]}\right] \quad (4)$$

where γ_{PB} and γ_{PS} are the volumetric coefficients of expansion of PB and PS respectively, and c_{PB} stands for the volume fraction of PB in the particle. For $c_{PB}=0.23$ which is characteristic for KRO-1 Resin, and for the following constituent properties of PB and PS:

$$K_{PB}=1.77\ \text{GPa}$$
$$K_{PS}=3.33\ \text{GPa}$$
$$E_{PS}=3.25\ \text{GPa}$$
$$\nu_{PS}=0.3$$
$$\gamma_{PS}=2\times10^{-4}\ \text{K}^{-1}$$
$$\gamma_{PB}=7.5\times10^{-4}\ \text{K}^{-1}$$

the particle properties given below can be obtained for room temperature.

$$K_P=0.861 \quad K_{PS}=2.87\ \text{GPa}$$
$$E_P=0.712 \quad E_{PS}=2.31\ \text{GPa}$$
$$\nu_P=0.335$$
$$\gamma_P=3.0\times10^{-4}\ \text{K}^{-1}$$

With this information the thermal stresses can be calculated readily from the concentric sphere solution as indicated above for a boundary condition of no radial traction in the outer surface. The result for the thermal misfit stresses, for a volume fraction $c_P=0.22$ of a particle phase and a temperature difference of $\Delta T=-75°C$ (from T_g of PS to room temperature) is

$$\sigma_{rr}=6.41\ \text{MPa}$$
$$\sigma_{00}=\sigma_{\phi\phi}=-5.64\ \text{MPa} \quad (5a,b)$$

at the border of the particle in the PS matrix.

Second, the additional stresses around the particles due to a superposed applied tension must be found. This is done by combining the classical solution of Goodier[21] (see also Mura[22]) for an isotropic sphere in an infinite medium with the particle interaction problem solved by Broutman and Panizza[23]. The computations of Boyce *et al.*[13] for these cases give the following stresses for a particle in an infinite medium.

$$\sigma_{rr}=0.05\,\sigma_\infty$$
$$\sigma_{00}=1.16\,\sigma_\infty$$
$$\sigma_{\phi\phi}=0.01\,\sigma_\infty$$

for an equatorial point A around the periphery of the particle in response to a distant tensile stress of σ_∞, as shown in *Figure 16*. The interaction solution of Broutman and Panizza[23] for a particle volume fraction of $c_P=0.22$ gives additional concentration factors of 1.133 for σ_{00} and about 2.0 for both σ_{rr} and $\sigma_{\phi\phi}$. Thus, considering the overall effect of distant stress in the presence of particle interactions

$$\sigma_{rr}=0.1\,\sigma_\infty$$
$$\sigma_{00}=1.314\,\sigma_\infty$$
$$\sigma_{\phi\phi}=0.02\,\sigma_\infty \quad (6a,b,c)$$

is obtained for the equatorial point A of *Figure 16*.

Spherical shell particle

Because of its special morphology the particles with concentric spherical shells of PB and PS with additional PB3K blended into the PB to a blend ratio of PB3K/KRO-1 of 0.5 require a numerical approach at all

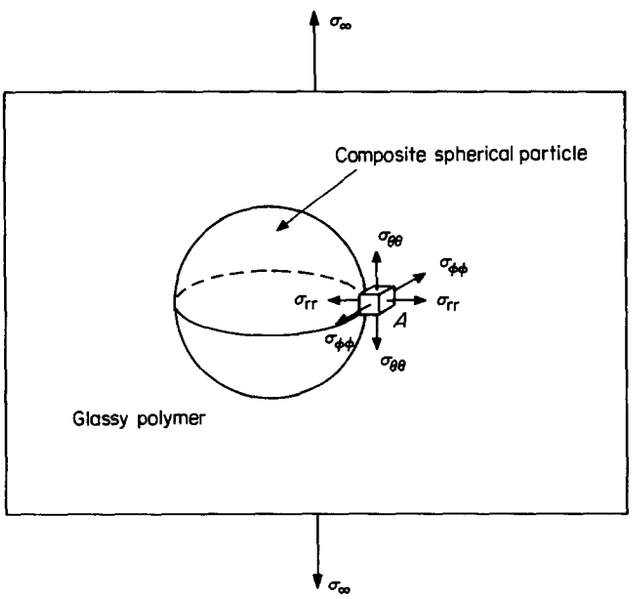

Figure 16 Equatorial point A around a spherical particle under a tensile stress, where craze initiation is most likely

levels. This has been done by Boyce *et al.*[13] in a way paralleling all the steps outlined for the KRO-1 particle above, by the use of finite element techniques. Their computations for a particle volume fraction of $c_P = 0.22$ has given thermal stresses at the periphery of the particles that are:

$$\sigma_{rr} = 11.413 \text{ MPa}$$
$$\sigma_{\theta\theta} = \sigma_{\phi\phi} = -10.236 \text{ MPa} \quad (7a,b)$$

On the other hand stresses at an equatorial point A due to a distant tension σ_∞ were found to be

$$\sigma_{rr} = 0.26\,\sigma_\infty$$
$$\sigma_{\theta\theta} = 1.194\,\sigma_\infty \quad (8a,b,c)$$
$$\sigma_{\phi\phi} = 0.092\,\sigma_\infty$$

which incorporate the same interaction amplification factors discussed above for the KRO-1 particle.

Craze initiation from particles

In the mechanistic crazing criterion of Argon and Hannoosh[24], crazes initiate in a local volume element when the following condition is satisfied

$$\frac{AQ}{(s/Y)} - \frac{3}{2}\left(\frac{\sigma}{Y}\right) = Q\ln(t/\tau) \quad (9)$$

In equation (9) σ is the negative pressure, s the deviatoric (shear) stress, Y the yield strength of the PS in tension, τ a time constant, A a material constant incorporating molecular parameters governing plastic flow, Q a numerical constant giving the ratio of the negative pressure for plastic expansion of a porous solid under a superposed large average deviatoric stress to the corresponding negative pressure when such an average deviatoric stress is absent, and finally t is the time for craze initiation measured from the time of the application of the stress. We recall that the deviatoric shear stress and the negative pressure are defined as

$$s = \sqrt{\tfrac{1}{6}[(\sigma_{rr}-\sigma_{\theta\theta})^2 + (\sigma_{\theta\theta}-\sigma_{\phi\phi})^2 + (\sigma_{\phi\phi}-\sigma_{rr})^2]} \quad (10)$$
$$= (\sigma_{rr} + \sigma_{\theta\theta} + \sigma_{\phi\phi})/3 \quad (11)$$

From extensive bi-axial craze experiments Argon and Hannoosh have determined that at room temperature $A = 9.54$, $Q = 0.0133$ and $\tau = 6 \times 10^{-8}$ s for PS, while the yield stress in tension $Y = 70$ MPa.

Evaluation of the crazing criterion of equation (9) for the stresses given in equations (5a,b) and (6a,b,c) for the KRO-1 particle and equations (7a,b) and (8a,b,c) for the spherical shell particles give $\sigma_\infty = 37$ MPa for the former and $\sigma_\infty = 28.3$ MPa for the latter at room temperature. These results are ranked in the appropriate order of high and low but do not compare well at all with the experimentally measured applied stresses of 30 MPa, and 10 MPa respectively.

Since the stress analysis of Boyce *et al.*[13] leaves very little room for uncertainty on the levels of local stress, we must conclude that the crazing criterion of Argon and Hannoosh[24], with its coefficients determined from experimental measurements on polystyrene homopolymer from quasi-uniform shear fields, is inapplicable to the surroundings of the composite particles. The use of more empirical crazing criteria advanced by others (for a discussion of their merits see Kawagoe and Kitagawa[25]) gives equally poor results. This all suggests that the previously developed craze initiation criteria, with their specific stress dependences that have been established for quasi-uniform stress fields, have the merit of coinciding with the results of a more general and yet undetermined formalism for craze initiation when applied to the types of problems previously investigated, but are not sufficiently general to explain the behaviour of crazing around the composite particle.

Nonetheless, the trends of the experiments and our stress analysis permit certain general observations. The craze initiating efficiency of a particle depends strongly on the thermal expansion misfit and difference of elastic properties between particles and matrix. The larger the effective coefficient of expansion of the particle and the more its elastic compliance relative to the matrix, the more effective is the craze initiation. In the blends prepared by us, the spherical shell particles with a PB3/KRO-1 ratio of 0.5 are the most effective in these two respects.

Comparing block copolymer blends with HIPS

High impact polystyrene has been one of a number of industrially important rubber-toughened polymers. A typical, commonly used HIPS contains grafted rubber at a weight fraction of 0.07–0.1. The particles have an average size at 2–4 μm and a moderately broad size distribution. In *Figure 17*, a tensile stress–strain curve is presented for a commercial HIPS in the form of a sheet of one millimeter thickness. The yield stress and modulus seem to be typical of any other specimen of HIPS manufactured for large scale use. The plastic strain-to-fracture may change in the range from 20% to 50%. One important and not widely recognized feature is that the films or sheets of HIPS often show an appreciable degree of notch sensitivity. In the samples tested, this does not seem to be a major feature. The HIPS particles consist of polystyrene occlusions surrounded by a topologically

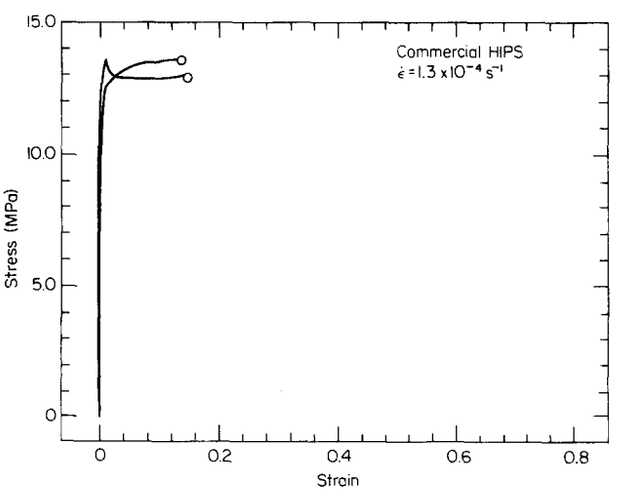

Figure 17 Typical stress–strain curve of a HIPS specimen strained at a rate of $1.3 \times 10^{-4}\,s^{-1}$ at room temperature

continuous minority phase of polybutadiene. They are connected by grafts to a matrix which is typically a high molecular weight and broad distribution polystyrene.

In the light of our blending studies, the effectiveness of the conventional HIPS particle also becomes clearer. The topologically continuous compliant rubbery phase imparts to the particle a high compliance that must be close to the lower bound estimate of the elastic stiffness for this composition. Furthermore, the success of Kruse[16] in increasing the toughness of conventional HIPS by blending additional PB into the particles is also clear. As was the case in our experiment, this incorporation of additional PB into the rubbery matrix of the particle increases both the compliance of the particle as well as its average thermal coefficient of expansion. We note that such improvement may be as advantageous as our results because they demonstrate that the toughness of glassy polymers can be dramatically improved well beyond what is normal practice with conventional HIPS.

ACKNOWLEDGEMENTS

This research has been supported by the NSF/MRL Program under Grant No. DMR 81-19295, through the Center for Materials Science and Engineering at MIT. We are also grateful to the Monsanto Polymer Products Company of Springfield, MA, for additional financial support that made a post-doctoral fellowship possible for O. S. Gebizlioglu, and for much additional help in providing polymers. We also acknowledge many stimulating discussions with our colleagues C. E. Schwier, M. E. C. Boyce and Prof D. M. Parks.

REFERENCES

1 Kambour, R. P. *J. Polym. Sci. Macromol. Rev.* 1973, **7**, 1
2 Bucknall, C. B. 'Toughened Plastics', Applied Science Publishers, London (1977)
3 Molau, G. E. *J. Polym. Sci., A* 1965, **3**, 1267
4 Molau, G. E. and Keskkula, H. *J. Polym. Sci., A-1* 1966, **4**, 1595
5 Riess, G. and Jolivet, Y. in 'Copolymer, Polyblends, Blends and Composites', Advances in Chemistry Series, ACS, Washington, D.C., Vol. 142, p. 243 (1975)
6 Echte, A. *Angew. Makromol. Chem.* 1977, **58–59**, 175
7 Kruse, R. L. *ACS Polym. Prepr.* 1977, **18**(1), 838
8 Gebizlioglu, O. S., Argon, A. S. and Cohen, R. E. *Polymer* 1985, **26**, 519
9 Bucknall, C. B. *J. Mater. Sci.* 1969, **4**, 214
10 Bucknall, C. B., Clayton, D. and Keast, W. E. *J. Mater. Sci.* 1972, **7**, 1443
11 Oxborough, R. J. and Bowden, P. B. *Phil. Mag.* 1973, **28**, 547
12 Oxborough, R. J. and Bowden, P. B. *Phil. Mag.* 1974, **30**, 171
13 Boyce, M. E. C., Argon, A. S. and Parks, D. M., to be published
14 Inoue, T., Soen, T., Hashimoto, T. and Kawai, H. in 'Block Copolymers', (Ed. S. L. Aggarwal), Plenum Press, New York, p. 73 (1970)
15 Kawai, H., Soen, T., Inoue, T., Ono, T. and Uchida, T. in 'Progress in Polymer Science—Japan', (Eds. K. Imahori and Y. Iwakura), Halsted Press, New York, Vol. 4, p. 145 (1972)
16 Kruse, R. L. US Patent 4154715 (1979)
17 Leibler, L. *Macromol. Chem., Rapid. Commun.* 1981, **2**, 393
18 Argon, A. S., Cohen, R. E., Gebizlioglu, O. S. and Schwier, C. E. in 'Advances in Polymer Science: Crazing in Polymers', (Ed. H. H. Kausch), Springer, Berlin, Vols. 52/53, p. 175 (1983)
19 Chow, T. S. *J. Polym. Sci. Polym. Phys. Edn.* 1978, **16**, 959
20 Chow, T. S. *J. Polym. Sci. Polym. Phys. Edn.* 1978, **16**, 967
21 Goodier, J. N. *ASME Trans.* 1933, **55**, 39
22 Mura, T. 'Micromechanics of Defects in Solids', Martinus Nijhoff, The Hague, Netherlands (1982)
23 Broutman, L. J. and Panizza, G. *Int. J. Polym. Mater.* 1971, **1**, 95
24 Argon, A. S. and Hannoosh, J. G. *Phil. Mag.* 1977, **36**, 1195
25 Kawagoe, M. and Kitagawa, M. *J. Polym. Sci. Polym. Phys. Edn.* 1981, **19**, 1423